

## **Low beta confinement in a Polywell modelled with conventional point cusp theories**

Matthew Carr, David Gummersall, Scott Cornish, and Joe Khachan

*Nuclear Fusion Physics Group, School of Physics A28, University of Sydney,  
NSW 2006, Australia*

(Dated: 11 September 2011)

The magnetic field structure in a Polywell device is studied to understand both the physics underlying the electron confinement properties and its estimated performance compared to other cusped devices. Analytical expressions are presented for the magnetic field in addition to expressions for the point and line cusps as a function of device parameters. It is found that at small coil spacings it is possible for the point cusp losses to dominate over the line cusp losses, leading to longer overall electron confinement. The types of single particle trajectories that can occur are analysed in the context of the magnetic field structure which results in the ability to define two general classes of trajectories, separated by a critical flux surface. Finally, an expression for the single particle confinement time is proposed and subsequently compared with simulation.

## I. THE POLYWELL CONCEPT

The Polywell fusion reactor is a hybrid device that combines elements of inertial electrostatic confinement (IEC)<sup>1-3</sup> and cusped magnetic confinement fusion<sup>4,5</sup>. In IEC fusion devices two spherically concentric gridded electrodes create a radial electric field that acts as an electrostatic potential well<sup>6-10</sup>. The radial electric field accelerates ions to fusion relevant energies and confines them in the central grid region. These gridded systems have suffered from substantial energy loss due to ion collisions with the metal grid. The Polywell concept<sup>11-16</sup> aims to replace the physical cathode with a virtual cathode that is formed by trapping energetic electrons in a magnetic cusp arrangement.

The Polywell's unique magnetic field configuration is created by pairs of opposing current loops, each creating a cusp. In the cube configuration each pair of loops is centred on a cartesian axis such that each loop sits on a face of the cube. The opposing contributions from each current loop cancel out in the centre of the device creating a magnetic null point. The resulting field acts like a magnetic well and a proportion of the electron population is confined by the magnetic mirror effect<sup>17,18</sup>.

By using a virtual cathode there is no longer a loss surface embedded within the plasma. The outer grid that contains the magnetic field coils is effectively isolated by the magnetic field it creates<sup>14</sup>. The field lines circulate around the coils and will deflect electrons from direct collisions. Instead they will tend to follow the field lines and re-circulate back into the device. The re-circulation mechanism may reduce the loss rate and improve the overall efficiency.

The cusp geometry utilised in the Polywell is known to be inherently magnetohydrodynamically stable because the field lines are everywhere convex toward the plasma<sup>19</sup>. However it may not be immune to kinetic instabilities such as the loss cone instability. The major energy loss mechanism is anticipated to be collisional scattering and direct propagation of electrons through the confining cusps.

The aim of this paper is to characterise the spatial structure of the magnetic field as a function of loop current, radius and loop spacing, in such a way that allows a detailed understanding of its underlying confinement properties. The trajectories of single electrons in this field structure will be analysed as representative of the confinement behaviour in a low-beta plasma where single particle behaviour may dominate. This information allows the

formation of a general model of confinement in the Polywell including predicted loss rates, and general guidelines for the construction of future experimental devices. Additionally, this model can be compared with other cusp systems as an indicator of relative performance and capability. Lastly, we derive an approximate expression for the magnetic fields in a simplified Polywell system for use in developing a more detailed theory.

## II. SIX POLYWELL CURRENT LOOPS

The full magnetic field in the Polywell can be obtained from the superposition of the contributions from each single current loop. For a single current loop centred on the origin of the  $z$  axis in cylindrical coordinates, the radial  $\rho$  and  $z$  axis components are<sup>21,22</sup>

$$B_\rho = \frac{\mu_0 I z}{2\pi} \sqrt{\frac{m}{4a\rho^3}} \left[ \frac{2-m}{2-2m} E(m) - K(m) \right] \quad (1)$$

$$B_z = \frac{\mu_0 I}{2\pi} \sqrt{\frac{m}{4a\rho^3}} \left[ \rho K(m) + \frac{am - \rho(2-m)}{2-2m} E(m) \right] \quad (2)$$

where

$$m = \frac{4a\rho}{z^2 + (a + \rho)^2} \quad (3)$$

The current in the loop is  $I$ , and  $a$  is the radius of the current loop. The functions  $E(m)$  and  $K(m)$  are the complete Elliptic integrals of the first and second kind respectively<sup>21</sup>.

The full magnetic field in the Polywell can be obtained from the superposition of the contributions from each loop. Since we are neglecting the higher order polywell geometries and limiting the analysis to the cube configuration we can make further use of the underlying symmetry in the device. Because each cartesian axis is orthogonal, each pair of loops centred on the same axis will contribute one of the  $B_\rho$  or  $B_z$  terms in a given cartesian coordinate, but never both. In a higher order geometry this would not be true and both terms would need to be considered. This can be shown by considering the six loop contributions to the total magnetic field in the  $\hat{\mathbf{x}}$  coordinate. Each coil has the two field contributions  $B_\rho$  and  $B_z$ , where  $B_z$  is now aligned with the axis on which each loop is centred. For the two loops centred on the  $\hat{\mathbf{x}}$  axis, each loop contributes a  $B_z$  term to the total field in the  $\hat{\mathbf{x}}$  direction. The radial  $B_\rho$  components of these two  $\hat{\mathbf{x}}$  axis loops are always perpendicular to the  $\hat{\mathbf{x}}$  axis, hence they make no contribution to the total field in the  $\hat{\mathbf{x}}$  direction.

The four off-axis loops (i.e. the two loop pairs centred on the  $\hat{y}$  and  $\hat{z}$  axes) have  $B_z$  contributions that are always perpendicular to the  $\hat{x}$  axis and hence are not included in the  $\hat{x}$  direction calculation. However each loop will have a  $B_\rho$  contribution to the  $\hat{x}$  axis. Consequently,  $B_\rho$  must be converted into cartesian coordinates. For example, the radial coordinate,  $\rho_{xz}$ , in the  $xz$  plane is given by  $\rho_{xz} = \sqrt{x^2 + z^2}$  which is used when obtaining the  $B_\rho$  contribution due to the loops on the  $\hat{y}$  axis. Therefore, in any given coordinate we expect to see two  $B_z$  terms from the two loops on the same axis, and four  $B_\rho$  terms from the four off axis loops. Thus, the equation for the Polywell field in the  $\hat{x}$  direction is

$$\begin{aligned} \vec{B}_x = & \left( B_z(\rho_{yz}, x - S) + B_z(\rho_{yz}, x + S) \right. \\ & + B_\rho(\rho_{xz}, y - S) \frac{x}{\rho_{xz}} + B_\rho(\rho_{xz}, y + S) \frac{x}{\rho_{xz}} \\ & \left. + B_\rho(\rho_{xy}, z - S) \frac{x}{\rho_{xy}} + B_\rho(\rho_{xy}, z + S) \frac{x}{\rho_{xy}} \right) \vec{\hat{x}} \end{aligned} \quad (4)$$

where  $B_z(\rho_{yz}, x - S)$  means the expression for  $B_z$  in Equation 2, with  $\rho_{yz}$  and  $x - S$  in place of the  $\rho$  and  $z$  coordinates respectively. The parameter  $S$  is the loop spacing parameter shown in Figure 1. The general expression for the overall magnetic field can be expressed as

$$\vec{B} = B_x \vec{\hat{i}} + B_y \vec{\hat{j}} + B_z \vec{\hat{k}} \quad (5)$$

where  $B_y$  and  $B_z$  are generated by cyclically permuting the coordinates in  $B_x$ , Equation 4.

### III. B FIELD STRUCTURE AND SINGLE PARTICLE TRAJECTORIES

The resultant magnetic field structure consists of field lines that enter through well defined point cusps in the loop faces and leave in the gaps between the loops. The magnetic field lines in the  $xy$  plane are shown in Figure 2. Note that the magnetic field is everywhere convex towards the centre of the device, making it inherently MHD stable<sup>11</sup>. Figure 3 shows the absolute value of  $\vec{B}$  in the  $xy$  plane, revealing its magnetic well structure. The magnitude of the magnetic field near the null point varies as  $r^3$  where  $r$  is the radius measured from the magnetic null point.

In principle electrons are confined by reflection from the point cusps if they are outside the loss cone<sup>14</sup>. However the motion is significantly complicated by the presence of the null point, which scatters the electrons' magnetic moment<sup>4</sup>. A sample electron trajectory is shown in Figure 4 where the electron is started in the centre of the device. Initially it is reflected from a point cusp in one of the faces but is then scattered around the null region in a chaotic way before eventually returning to its starting point. Figure 5 shows the superposition of 10 such trajectories with randomised starting positions and calculated until they leave the cube region defined by the six Polywell loops.

The motion shown in Figures 4 and 5 is only a slightly more complicated version of the motion in the comparatively simpler biconic cusp. Theories of biconic cusp confinement are based on the hypothesis that there exists a critical flux tube separating an outer region of completely adiabatic orbits from an inner region where every field line passes through a distinctly non-adiabatic region<sup>5,23,24</sup>. Orbits guided by magnetic field lines of the latter type consist of segments of adiabatic motion near the reflection points, separated by a non-adiabatic portion which randomises the magnetic moment. This hypothesis and the underlying confinement theory derived from it can be extended to apply to the Polywell magnetic field geometry.

The motion of electrons originating in the centre can be understood by examining the behaviour of the electron gyroradius as a function of radius from the central null point. In the vicinity of the null point the gyroradius changes rapidly. Over a distance of half the device radius, the gyroradius  $r_g$  can change from  $\infty$  to  $\approx 1\text{cm}$ . This leads to almost straight trajectories in the centre of the magnetic well until the electron is turned around at a region of high field where  $r_g$  approaches 10% of the device radius.

Electrons will be reflected inside the low field region until they eventually enter a point cusp where the magnetic field is directed radially outwards. As a consequence of this change in field geometry, the electrons follow the field lines out of the device. Additionally, there is a transition to a region where the magnetic field changes slowly compared with the electron gyroradius and the magnetic moment,  $\mu$ , becomes an adiabatic constant of motion. At this point the electron motion is completely adiabatic and is reflected if the peak magnetic field  $B_{peak} > \text{kinetic energy}/\mu$ <sup>18</sup>. The magnetic moment of the electron will be scattered each time it passes through the non-adiabatic region. Consequently, no electron with this class of trajectory will be confined indefinitely because it will eventually be scattered into a loss

cone.

The boundary that separates adiabatic and non-adiabatic segments of motion is described by the condition for adiabatic invariance of the magnetic moment<sup>18</sup>:

$$r_g \left| \frac{\nabla B}{B} \right| \ll 1 \quad (6)$$

This transition is not sharply defined, but occurs over a finite distance. However for the purposes of this analysis, we have chosen to approximate the transition region by the contour of  $r_g = 0.1R$ , where  $R$  is the device radius.

The critical flux tube is defined as the set of magnetic field lines that have their minimum magnetic field point on the adiabatic boundary<sup>23,24</sup>, which is shown as the gray contour in Figure 6. A sample trajectory is shown for the case where the electron is started inside the critical flux tube. It has clearly defined segments of adiabatic and non-adiabatic motion. For electrons started outside this flux surface, the motion is completely adiabatic and the electron will be confined to a given field line. If the peak magnetic field along the field line is  $B_{peak} > KE/\mu$ , the electron will be confined indefinitely. Because the magnetic field is not uniform the electrons will drift on the same flux surface around the point cusp. This drift motion is shown in Figure 7.

#### IV. POINT AND LINE CUSPS

Despite having favourable MHD stability properties, the major disadvantage of open-ended minimum B geometries is the rapid loss of plasma through their loss gaps. The biconic cusp geometry has two point cusps along the central axis and a wide ring cusp in the central plane of symmetry<sup>4</sup>. Some mirror devices utilise Joffe bars to create a cusp that stabilises the interchange instabilities<sup>25</sup>. However the cusp in this type of device has wide linear loss gaps between the bars. It has been found that linear loss gaps, here referred to as line cusps, considerably reduce the effectiveness of plasma confinement and form the dominant loss mechanism from the device<sup>26</sup>. Various attempts to plug the line cusp have included electrostatic repeller plates, RF power, and simultaneous injection of plasma through the line cusp<sup>27</sup>. However none of these attempts have succeeded in adequately reducing the rate of loss from the line cusps.

The high-order spherical multipole was developed as a minimum B field configuration

that eliminates the line cusps and consists only of point cusps<sup>26</sup>. Experimental studies compared a multipole field consisting of 30 point cusps with a conventional spindle cusp and found that the confinement time was 2.5 times longer in the multipole field<sup>28</sup>. Although the experiment succeeded in eliminating the line cusps, the overall loss rate is proportional to the number of individual point cusps, and hence only led to a marginal improvement in overall confinement. The unique field geometry in the Polywell appears to solve both problems.

The point cusps in each face of the Polywell can be analysed with the conventional theory of cusp losses. However the structure of the loss region between the coils is far more complicated and was referred to by Bussard as the “funny cusp”<sup>14</sup>. By analysing the magnitude of the magnetic field at two crucial points we will show that this region can be treated as eight separate point cusps if the loop spacing,  $S$ , is less than a critical distance.

The simplest starting point is the case where the current loops are all in contact,  $S = a$ . The peak magnetic field in the face point cusp is given by taking the limit of Equation 4 as  $y$  &  $z = 0$ , and  $S$  &  $x = a$ .

$$\lim_{\substack{y,z \rightarrow 0 \\ S,x \rightarrow a}} B_x = \frac{\mu_0 I \left( (\sqrt{5} - 25)\pi + 20\sqrt{5} \left( 3E\left(\frac{4}{5}\right) - K\left(\frac{4}{5}\right) \right) \right)}{50a\pi}$$

$$\therefore B_{face} \approx \frac{0.286\mu_0 I}{a\pi} \quad (7)$$

This equation is similar to the standard equation for the field due to a current loop<sup>20</sup>, except with an additional constant term that effectively describes the field reduction due to the superposition of the other adjacent current loops. Let us now express the loop spacing in terms of the loop radius,  $a$ , through a dimensionless parameter  $s$ , where  $S = sa$ . If the spacing parameter  $s$  is now allowed to vary, we expect that  $B_{face}$  must have the same form as equation 7 but multiplied by a function of  $s$  that describes the changing superposition of the other loop components. We have found from numerical methods that it can be approximated by a log dependence on  $s$ .

$$B_{face}(s) = \frac{0.286\mu_0 I}{a\pi} 2 \log[10.56(s - 0.85)] \quad (8)$$

By similar analysis the corner cusp is expressed as

$$B_{corner}(s) = \frac{\mu_0 I}{a\pi} \left( \frac{1}{5.7(s - 0.88)} \right) \quad (9)$$

The field in the edge line cusp is dominated by the two closest loops. When these are almost in contact, we can approximate them as two infinitely straight wires. The expression for the field due to a straight wire is<sup>20</sup>

$$B_{stright}(r) = \frac{\mu_0 I}{2\pi r} \quad (10)$$

where  $r$  is the distance from the wires. In the geometry of the polywell, it can be shown that

$$r = \frac{a(s-1)}{\sqrt{2}} \quad (11)$$

We have found that Equation 10 approximates the numerically calculated data, providing allowance is made for an extra fitted geometrical factor, which takes into account the field reduction due to cancellation with the four more distant current loops.

$$B_{edge}(s) = \frac{\mu_0 I}{2\pi} \frac{\sqrt{2}}{a(s-1)} 0.81 \quad (12)$$

Figure 8 shows the variation of  $B_{face}$ ,  $B_{corner}$  and  $B_{edge}$  as a function of the spacing parameter  $s$ . The underlying trend of field variation with spacing is dominated by the behaviour of the nearest coil components. For example, the  $B_{face}$  field is substantially reduced due to cancellation with the fields produced by the adjacent coils, and this effect is strongest at small spacings. In contrast, both  $B_{corner}$  and  $B_{edge}$  originate from the constructive addition of the adjacent coil components and result in an increase in field strength with reduced spacing.

At small loop spacings the magnetic field in the centre of the line cusp,  $B_{edge}$ , is almost an order of magnitude larger than the field in both types of point cusps. Consequently, in the region of small loop spacing the losses due to the point cusps will dominate, while ignoring the more complicated line cusp components. Instead the loss rate can be modeled with 14 point cusps - 6 due to the faces and 8 due to the corners. This point is reinforced in the heat map of magnetic field strength in Figure 9, revealing “the funny cusp” region can be modeled as a point cusp.

The fact that the line cusp component can be neglected indicates that the Polywell magnetic field geometry might result in a greater confinement time than the conventional biconic cusp. In the biconic cusp, the situation is reversed and the line cusp losses dominate<sup>26</sup>. Figure 10 shows contour plots for the magnetic field in the  $xy$  plane of both devices. The

biconic cusp has a wide linear loss region in the central plane of rotation. Here the field is substantially lower than the point cusp, and when revolved in 3D, the loss area is very large. By comparison, because the line cusps can be ignored in the Polywell, the point cusp losses dominate and we expect the loss rate is substantially lower. Consequently confinement times should be longer in the Polywell field geometry.

## V. CENTRAL MAGNETIC FIELD APPROXIMATION

In order to assess the future of the Polywell concept as a fusion energy device and further improve our understanding of its limitations we seek a model system that sufficiently captures the essential physics of the Polywell, while simultaneously being simple enough to make theoretical calculations tractable. For example, in order to carry out an analysis of the electron confinement time in the central region of the Polywell, we need to obtain an unsophisticated analytical expression in closed form for the magnetic field in this region.

For situations of high cylindrical symmetry, the axial magnetic field components of a single loop,  $B_\rho$  and  $B_z$ , can be approximated near the axis of symmetry in terms of the field along the  $z$  axis only<sup>29</sup>,

$$\begin{aligned} B_\rho(\rho, z) &= -\frac{\rho}{2}B'_z(z) + \frac{\rho^3}{16}B_z'''(z) - \dots \\ &= \sum_{n=1}^{\infty} \frac{(-1)^n B_z^{2n-1}}{n!(n-1)!} \left(\frac{\rho}{2}\right)^{2n-1} \end{aligned} \quad (13a)$$

$$\begin{aligned} B_z(\rho, z) &= B_z(z) - \frac{\rho^2}{4}B_z''(z) + \dots \\ &= \sum_{n=0}^{\infty} \frac{(-1)^n B_z^{2n}}{(n!)^2} \left(\frac{\rho}{2}\right)^{2n} \end{aligned} \quad (13b)$$

Hence, the contributions due to the two loops centred on a single cartesian axis can be described by their superposition along that axis only. The magnetic field along the axis of a single coil is<sup>20,22</sup>

$$B_z(z) = \frac{\mu_0 I a^2}{2(a^2 + z^2)^{3/2}} \quad (14)$$

and thus the contributions to the field by these two coils are the sum of two  $B_z(z)$  axial equations centred on offsets of  $\pm S$ . In the interests of simplicity let us limit the analysis to

the case where adjacent coils are in contact,  $S = a$  (or equivalent to  $s = 1$ ), and expand these axial terms in a Taylor series about the point  $z = 0$ . To avoid a non-trivial solution we need to take terms to third order. This results in

$$B_z(z) \approx \frac{\mu_0 I z (24a^2 + 5z^2)}{32\sqrt{2}a^4} \quad (15)$$

This series approximation converges very well in the region  $\pm a/2$ , thus the simplified model system will only accurately reflect the field structure in the core of the Polywell. Substituting Equation 15 into Equations 13a and 13b, and using the results in Equations 4 and 5 yields

$$\begin{aligned} \vec{B} = & \frac{35\mu_0 I}{128\sqrt{2}a^4} \left( (-2x^3 + 3x(y^2 + z^2))\vec{x} \right. \\ & \left. + (-2y^3 + 3y(x^2 + z^2))\vec{y} + (-2z^3 + 3z(x^2 + y^2))\vec{z} \right) \end{aligned} \quad (16)$$

The resultant field lines in the  $xy$  plane are shown in Figure 11. Bussard's original field approximation,  $B \propto r^3$ , can be recovered by setting  $y = z = 0$  in Equation 16, which gives the field along the  $\vec{x}$  axis,  $B_x \propto x^3$ .

Future analysis of plasma dynamics within the Polywell may require closed form expressions of the magnetic vector potential  $\vec{A}$ . This can be obtained by using the same methods shown here for the magnetic field,  $\vec{B}$ , by using the same on-axis approximation for two loops with opposing currents. Zworykin<sup>29</sup> presents an approximation for  $\vec{A}$  derived from Stoke's theorem and Maxwell's equations. In the special case of two loops centred on the same axis with high cylindrical symmetry,  $\vec{A}$  only has components in the direction of  $\vec{\theta}$ .

$$\begin{aligned} A_\theta(\rho, z) &= \frac{\rho}{2} B_z(z) - \frac{\rho^3}{16} B_z''(z) + \dots \\ &= \sum_{n=0}^{\infty} \frac{(-1)^n B_z^{2n}}{n!(n+1)!} \left(\frac{\rho}{2}\right)^{2n+1} \end{aligned} \quad (17)$$

Using Equation (15) in the approximation for  $\vec{A}$  gives:

$$A_\theta(\rho, z) = -\frac{\mu_0 I \rho z (96a^2 + 20z^2 - 15\rho^2)}{256\sqrt{2}a^4} \quad (18)$$

Summing the contributions from each axis and using similar geometric arguments gives the expression for the total  $\vec{A}$ .

$$\vec{A}_x = A_\theta(\rho_{xy}, z) \frac{y}{\sqrt{x^2 + y^2}} - A_\theta(\rho_{xz}, y) \frac{z}{\sqrt{x^2 + z^2}} \quad (19)$$

Using the two loop approximation (Equation 15) we find the  $\vec{x}$  axis term,

$$\vec{A}_x = \frac{35\mu_0 I y z (y^2 - z^2)}{256\sqrt{2}a^4} \quad (20)$$

The other components of  $\vec{A}$  can be generated by cyclically permuting the cartesian coordinates in Equation 20. In Figure 12 a sample flux surface is shown by plotting the region  $\vec{A} = \text{constant}$ . The adiabatic trajectory shown in Figure 7 is constrained to a flux surface like the example shown in this figure.

## VI. APPROXIMATE LOSS RATE AND CONFINEMENT TIME

The simplified expressions for  $\vec{B}$  in Equation 16 can be used to create and test an approximate model of electron confinement in the Polywell. These equations apply to the limit of small spacing where the loops are in contact, and the contributions of the line cusps can be ignored. The fraction of the electron population inside the loss cone of a single point cusp is well established<sup>18,30</sup>. Bussard argued that this fraction can be modified by a factor of  $n$  for a system of  $n$  point cusps that do not have overlapping loss cones<sup>31</sup> given by

$$L = \frac{n}{2} \left( 1 - \sqrt{1 - \frac{B_0}{B_m}} \right) \quad (21)$$

In this case there are  $n = 14$  point cusps (6 due to the faces and 8 from the corners). The magnetic field,  $B_0$ , is the minimum field from which the magnetic moment is conserved and occurs at the radius  $r_0$ . The peak magnetic field in the device is  $B_m$ . For the population of electrons inside the critical flux surface, the loss fraction can be interpreted as the probability of escape after each successive random scattering event inside the central non-adiabatic region. Therefore, by ignoring the influx of electrons from external sources, the loss rate of electrons escaping from the magnetic well can be expressed as

$$\frac{dN(t)}{dt} = -\frac{LN}{\tau_{trans}} \quad (22)$$

$$\therefore N(t) = N_0 e^{\frac{-Lt}{\tau_{trans}}} \quad (23)$$

where  $N(t)$  is the number of electrons remaining after a time  $t$  of being introduced into the central region.

The average transit time  $\tau_{trans}$  can be approximated by considering both the adiabatic and non-adiabatic components of the electron trajectories. The non-adiabatic components consist of approximately straight trajectories that are randomly scattered about the well until they enter a point cusp. As an order of magnitude estimate, we have assumed without further analysis an average of 10 scattering events before entering a loss cone. This assumption is only based on observing the statistics of the numerically calculated trajectories.

The transit time along a point cusp in the adiabatic mirror region can be found by considering the change in parallel velocity as the electrons move into stronger field regions<sup>30</sup>. The velocity component parallel to the magnetic field,  $v_{\parallel}$ , can be expressed in terms of the initial velocity  $v_0$  and the mirror ratio  $B(z)/B_0$  as

$$v_{\parallel} = v_0 \sqrt{1 - \frac{B(z)}{B_0} \sin^2 \theta_0} \quad (24)$$

where  $\theta_0$  is the angle between the velocity vector and the magnetic field at  $B_0$ . Since  $v_{\parallel} = \frac{dz}{dt}$ , it can be shown that

$$t = \frac{1}{v_0} \int \sqrt{1 - \frac{B(z)}{B_0} \sin^2 \theta_0} dz \quad (25)$$

Therefore, the total transit time in the Polywell between adiabatic reflections is the sum of the transit times on either side of the critical flux tube.

$$\tau_{trans} = \frac{2}{v_0} \int \sqrt{1 - \frac{B(z)}{B_0} \sin^2 \theta_0} dz + 2 \frac{10r_0}{v_0} \quad (26)$$

This model was tested in the Simion charged particle optics package<sup>32</sup>. The starting position of 10,000 electrons were randomly distributed in a central spherical region inside the critical flux surface. Hence only electrons with two-component trajectories were studied. Other parameters were chosen to match previous<sup>33</sup> or planned experimental studies. All electrons had an initial energy of 100eV, and the current in the loops was 10kA. The current loop radius was set at 0.025m. The electron trajectories were calculated until they left the cube region defined by the Polywell coils, i.e. a cube with side length 0.05m centred on the origin. The confinement time of each electron was recorded and the resulting distribution is

shown in Figure 13.

The simulation was compared with the model predictions in Equation 26 and the magnetic fields were calculated directly with the simplified central well Equation 16. Hence the model was tested against the simplest magnetic field case. The minimum magnetic field at which the magnetic moment is conserved,  $B_0$ , was calculated from the critical flux tube where  $r_g = 10\%R$ . The angle with the deepest penetration in to the cusp field was used for  $\theta_0$ . All other parameters were as given above in the simulation.

The fit to the simulated data (solid line) and the theoretical calculation (dashed line) is found to be in good agreement. The exponential decay of the simulated data confirms that a statistical scattering model is relevant inside the critical flux tube. The simulated data was found to have a mean confinement time of  $\tau_0 = 0.129\mu s$ , compared with a theoretically calculated value of  $\tau_0 = 0.163\mu s$ . It is worth pointing out that no effort has been made to adjust the input parameters to optimise the confinement time. The input values used only represent a single case used to test the applicability of conventional point cusp theory.

## VII. ELECTROSTATIC PLUGGING OF POINT CUSPS

The prospect of the Polywell as a fusion energy device has to be examined within the context of a sub-microsecond confinement time. For example, a litre of 100eV electrons at a density of  $10^{19}\text{m}^{-3}$  would require  $\approx 400\text{kW}$  of input power to sustain the energy lost by the electrons with  $\tau_0 \approx 0.15\mu s$ . However the model developed in this paper is only intended to accurately describe the low beta case (such as during startup) and at higher densities other plasma effects are anticipated to increase the confinement time.

Space charge limited flow could occur along the critical flux tube, effectively plugging the point cusps. Each point cusp can be treated as an isolated flux tube and modeled like a vacuum diode with the Child-Langmuir law. The electron current leaking from the polywell along a point cusp in Figure 12 is similar to the electron current emitted by the cathode in a vacuum diode. The Child-Langmuir law for space charge limited current is

$$j = \frac{4}{9}\epsilon_0\sqrt{\frac{2e}{m_e}}\frac{V^{3/2}}{h^2} \quad (27)$$

where  $V$  is the voltage applied to plane electrodes separated by a distance  $h$ <sup>34</sup>. In the case of a virtual cathode forming in the middle of the polywell, the anode to virtual cathode

voltage may be  $\approx 100\text{V}$  for  $100\text{eV}$  electrons. Taking a worst case scenario approach, the point cusp leakage area can be estimated as roughly the geometric size of the critical flux tube, giving a radius on the order of  $0.5\text{cm}$ . After taking into account the total leakage area for all 14 point cusps and assuming  $h \approx 0.5\text{cm}$ , we find  $I \approx 0.1\text{A}$  or equivalently  $10\text{W}$  of power lost. Obviously this calculation is far too simplistic to be accurate because space charge effects have been neglected, but it does demonstrate the concept of electrostatically plugging the cusps. These effects could be included in future studies by consulting Dolan's review article on electrostatic cusp plugging<sup>15</sup>.

## VIII. CONCLUSIONS

The magnetic field structure of the Polywell has been analysed in its complete form, as well as areas of interest such as the point and line cusps, and the central well approximation. It has been found that at small spacings it is possible for point cusp losses to dominate over line cusp losses, allowing the application of conventional point cusp theory to the Polywell. The dominance of point cusp losses may prove beneficial in terms of providing a lower overall loss rate when compared with other devices such as the biconic cusp.

The types of trajectories that can occur have been analysed in terms of their adiabaticity. It was found that the two component trajectories described in models of biconic cusp confinement can be adapted to the Polywell. The resulting model describes a critical flux surface separating the two types of trajectories, and also defines the minimum field,  $B_0$ , needed for a simple scattering model of confinement.

The simplified scattering model was found to be in reasonable agreement with a simulation with parameters matching our current experimental parameters. The central well approximation was used to calculate magnetic fields for the model and simulations, but the correlation between these and experimental results will be left for future work. Future studies should address the question to what degree confinement in the Polywell is determined by the parameters of the central well field, and whether the central well approximation can be used to study other aspects of Polywell plasma physics. Furthermore, the model of point cusp loss needs to be extended for the high beta case where electrostatic plugging is anticipated to have a favourable effect on the overall electron confinement time.

## REFERENCES

- <sup>1</sup>P. T. Farnsworth, U.S. Patent No. 3,258,402 (1966).
- <sup>2</sup>P. Farnsworth, Method and apparatus for producing nuclear-fusion reactions, (1968), US Patent 3,386,883.
- <sup>3</sup>R. Hirsch, J. Appl. Phys. **38**, 4522 (1967).
- <sup>4</sup>J. Berkowitz et al., Proceedings of the 2nd Int. Conference on Peaceful Uses of Atomic Energy. **1**, pages 146-155 (1958).
- <sup>5</sup>H. Grad, Physical Review Letters **4**, 222 (1960).
- <sup>6</sup>W. Elmore, J. Tuck, and K. Watson, Phys. Fluids **2**, 239 (1959).
- <sup>7</sup>O. A. Lavrentev, Ukr. Fiz. Zh. **8**, 440 (1963).
- <sup>8</sup>R. L. Hirsch, Phys. Fluids **11**, 2486 (1968).
- <sup>9</sup>G. H. Miley, J. Nadler, T. Hochberg, Y. Gu, O. Barnouin, and J. Lovberg, Fusion Technol. **19**, 840 (1991).
- <sup>10</sup>J. Khachan, and S. Collis, Phys. Plasmas **8**, 1299 (2001).
- <sup>11</sup>R. Bussard, Fusion Technol. **19**, 273 (1991).
- <sup>12</sup>N. Krall, Fusion Technol. **22**, (1992)
- <sup>13</sup>N. Krall, M. Coleman, K. Maffei, J. Lovberg, R. Jacobsen, and R. Bussard, Phys. Plasmas **2**, 146 (1995).
- <sup>14</sup>R. Bussard, in *57th International Astronautical Congress*, IAC (2006).
- <sup>15</sup>T. Dolan, Plasma Physics and Controlled Fusion **36**, 1539 (1994).
- <sup>16</sup>J. Santarius and K. Simmons, 1995 IEEE International Conference on Plasma Science, 1995. IEEE Conference Record-Abstracts, (1995).
- <sup>17</sup>R. Post, Nucl. Fusion **27**, 1579 (1987).
- <sup>18</sup>F. Chen, *Introduction to plasma physics and controlled fusion*, Vol. 1 (Plenum press, 1984).
- <sup>19</sup>J. Berkowitz, H. Grad, and H. Rubin, Proceedings of the 2nd Int. Conference on Peaceful Uses of Atomic Energy. **1**, pages 177-189, (1958).
- <sup>20</sup>D. Griffiths and C. Inglefield, *Introduction to electrodynamics*, (1999), Prentice Hall New Jersey.
- <sup>21</sup>R. Good, European Journal of Physics **22**, 119 (2001).
- <sup>22</sup>J. Jackson, *Classical electrodynamics, 2nd Ed*, (1975), John Wiley and Sons.
- <sup>23</sup>H. Grad, *Containment in Cusped Plasma Systems*, New York Univ., New York. Inst. of

- Mathematical Sciences (1961).
- <sup>24</sup>R. Van Norton, *The motion of a charged particle near a zero field point*, New York Univ., New York. Inst. of Mathematical Sciences (1961).
- <sup>25</sup>L. Artsimovich, *Controlled Thermonuclear Reactions*, (Gordon and Breach, 1964).
- <sup>26</sup>M. Sadowski, *Physics Letters A* **25**, 695 (1967).
- <sup>27</sup>S. Glasstone and R. Lovberg, *Controlled thermonuclear reactions: an introduction to theory and experiment*, (RE Krieger Pub. Co., 1960).
- <sup>28</sup>M. Sadowski, *Journal of Plasma Physics* **4**, 1 (1970).
- <sup>29</sup>V. Zworykin, G. Morton and E. Ramberg, *Electron Optics and the Electron Microscope*, John Wiley and Sons, Inc., New York (1945).
- <sup>30</sup>D. Rose and M. Clark, *Plasmas and controlled fusion*, The MIT Press, Cambridge, Massachusetts (1961).
- <sup>31</sup>See National Technical Information Service Document No. ADA257648. (R. Bussard and N. Krall, EMC2 Technical Report 0191-02, Feb 1991). Copies may be ordered from the National Technical Information Service, Alexandria, VA 22312.
- <sup>32</sup>D. Dahl, *Int. J. Mass Spectrom.* 200 (2000) 3. (source: Scientific Instrument Services, Inc., Ringoes, NJ, [www.simion.com](http://www.simion.com))
- <sup>33</sup>M. Carr and J. Khachan, *Physics of Plasmas* **17**, 052510 (2010).
- <sup>34</sup>M. Lieberman and A. Lichtenberg, *Principles of plasma discharges and materials processing*, John Wiley and Sons, Inc., New York (1994).

## FIGURES

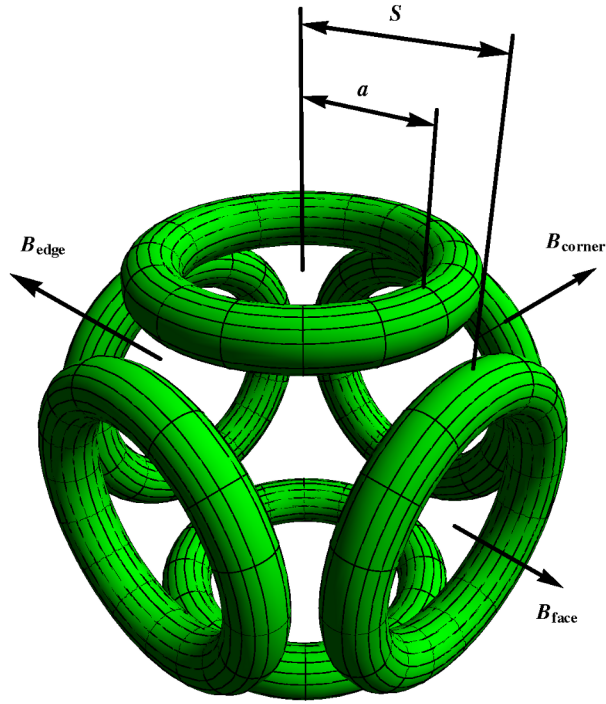


FIG. 1. A diagram of the cube polywell configuration. The coil radius  $a$  and coil spacing  $S$  are marked. Vectors have been used to indicate the positions of the Face, Corner and Edge regions.

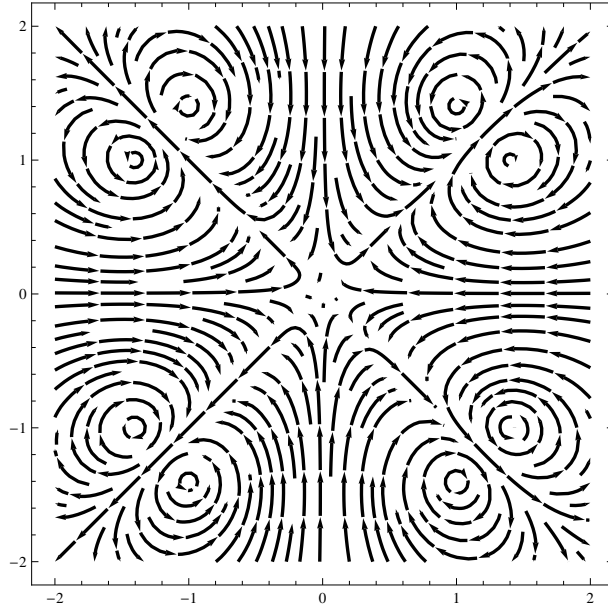


FIG. 2. The magnetic field lines in the  $xy$  plane intersecting four of the six coils. In this plane there are four point cusps, one centred on each coil face. These have been labeled as face cusps. Also present are four line cusps, one in each corner in the spacing between the coil windings. These have been labeled as edge cusps.

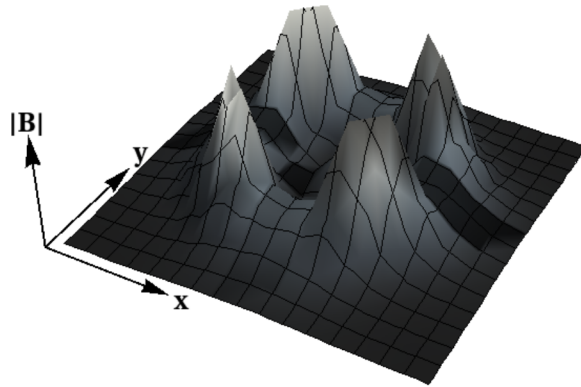


FIG. 3. The magnitude of the magnetic field in the same  $xy$  plane as in Figure 2. It is clear from this structure that the Polywell creates a magnetic well.

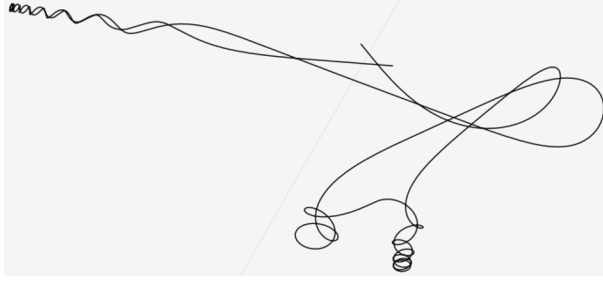


FIG. 4. A sample isolated electron trajectory. The electron was initialised at the centre of the device with an energy of 100eV and a randomised velocity vector. The current loops are not drawn in the background so as to clarify the different types of motion present. The electron has a clearly defined magnetic moment in three places where it is reflected from a high field region. In the central region it has smoother trajectories.

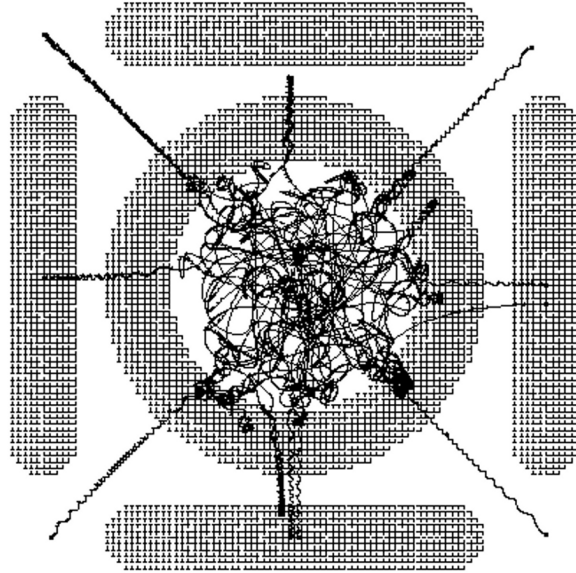


FIG. 5. A superposition of 10 different electron trajectories. Each electron has a starting energy of 100eV and a randomised position and directed velocity. The trajectories are plotted until the electrons reach the coil's cube surface, at which point they are considered lost.

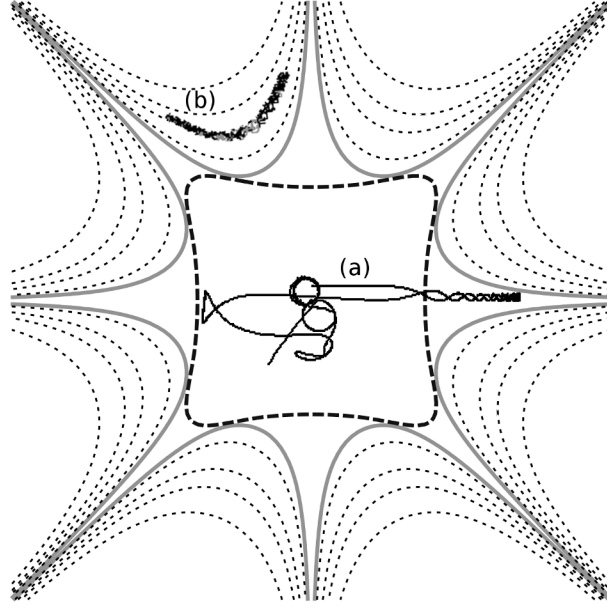


FIG. 6. The critical flux surface separating the two types of trajectories is shown as the thick gray line. The dashed line is the contour where the gyroradius is 10% of the device radius. Other example field lines are shown as dotted lines. Trajectory (a) is inside the critical flux surface and consists of regions of adiabatic motion separated by random scattering in the central non-adiabatic region. Trajectory (b) is completely adiabatic and is confined indefinitely.

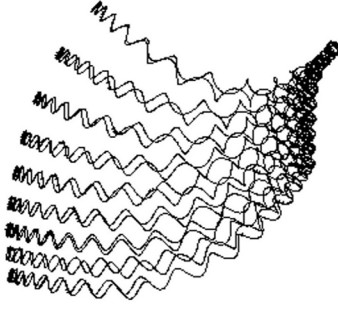


FIG. 7. A 3D isometric view of the single trajectory shown in Figure 6 (b). The motion is completely adiabatic and will be confined indefinitely. Because the magnetic field is not completely uniform the electron drifts on a constant flux surface around the point cusp. When the motion is projected into the  $xy$  plane (as in Figure 6) the trajectory is clearly confined to a constant set of field lines.

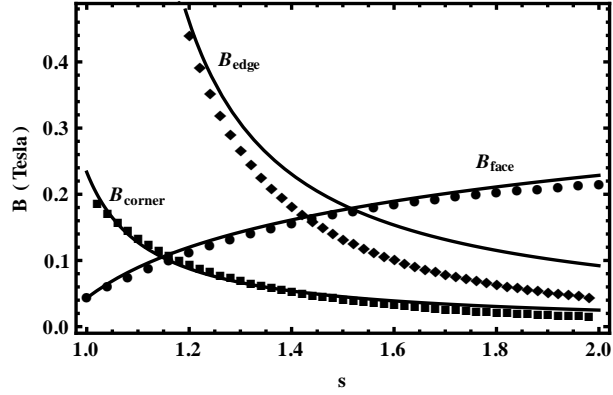


FIG. 8. The field strength in the face, corner and edge cusps plotted together. The approximate equations for these different field regions described in the text are shown as solid lines, compared with numerically calculated data points. It is significant that at small loop spacings, the line cusp field is almost an order of magnitude larger than the point cusp components.

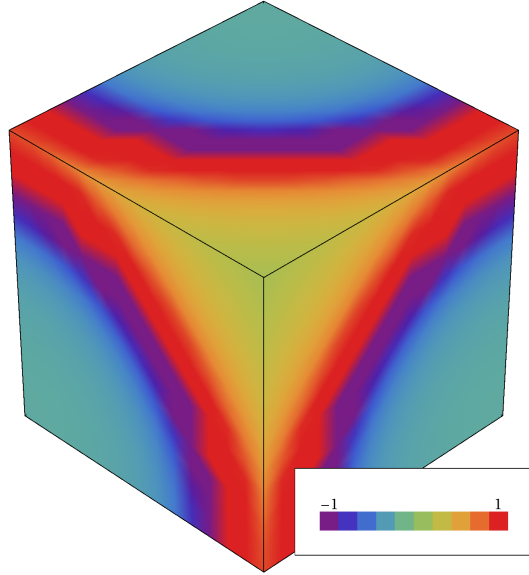


FIG. 9. (Color) The relative magnitude and sign of the radial magnetic field  $B_r \vec{r}$  on the cube surface containing the current loops. Only 1/8th of the surface is shown to reveal the smallest symmetrical element in detail. Blue and purple areas of the surface indicate where the field diverges radially and reveal the point cusp structure of the face cusps. The yellow and red areas show radial convergence of the field and hence reveal the “funny cusp” region described by Bussard. However, since the strongest field is present in the edge cusp near the current loops, this region can be neglected. Instead the funny cusp region can be modeled by only considering the corner cusp component as a point cusp.

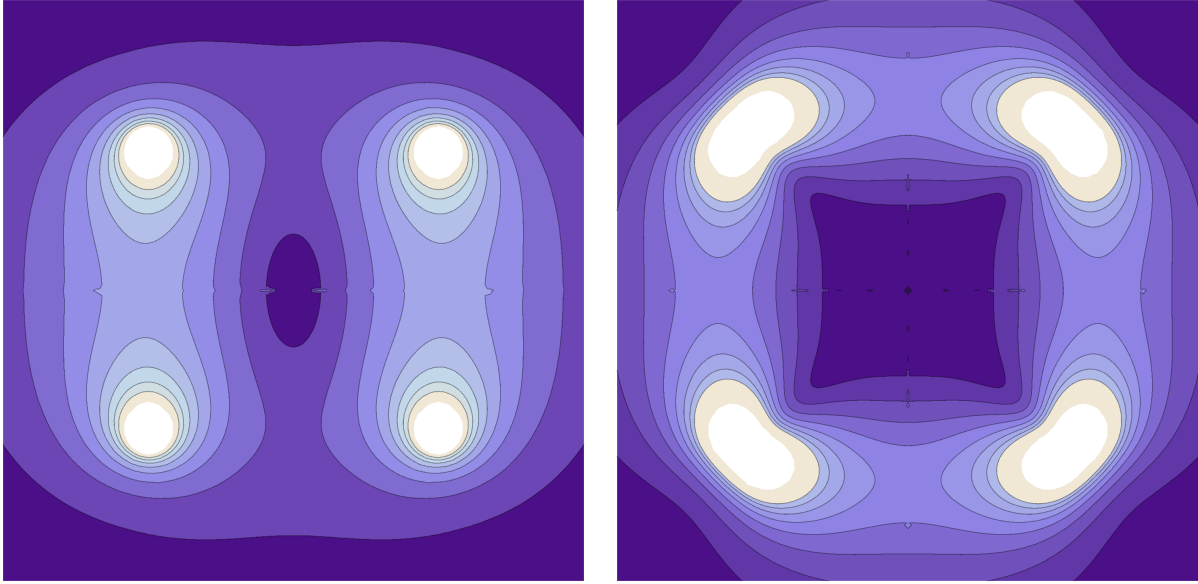


FIG. 10. (Color online) A comparison of a biconic cusp (top) and the Polywell (bottom) magnetic fields. Both plots show contours of magnetic field strength in the  $xy$  plane. Eight contours are plotted ranging from 0.025T to 0.2T in steps of 0.025T. The darkest contour shading represents the region of lowest magnetic field, through to white for the highest field region. The current in the biconic cusp has been adjusted so that the peak field in the face point cusp of both devices is equal, allowing comparison of the two confining magnetic field structures. In the biconic cusp, the field in the circular line cusp is clearly much weaker than in the point cusp. The line cusp losses dominate both because the field is weaker in this region, and also because the loss area is much larger when revolved around the symmetry axis. In the Polywell, this situation is reversed and the point cusps exhibit the weakest magnetic field.

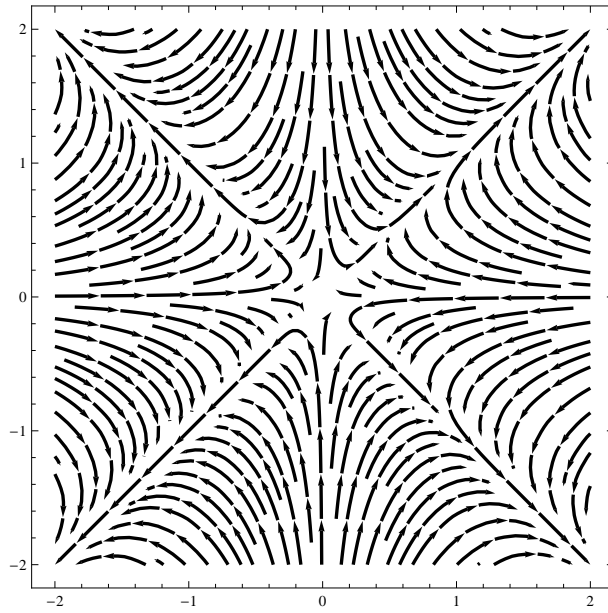


FIG. 11. The fieldlines generated by Equation 16. This field closely approximates the interior magnetic field of the Polywell.

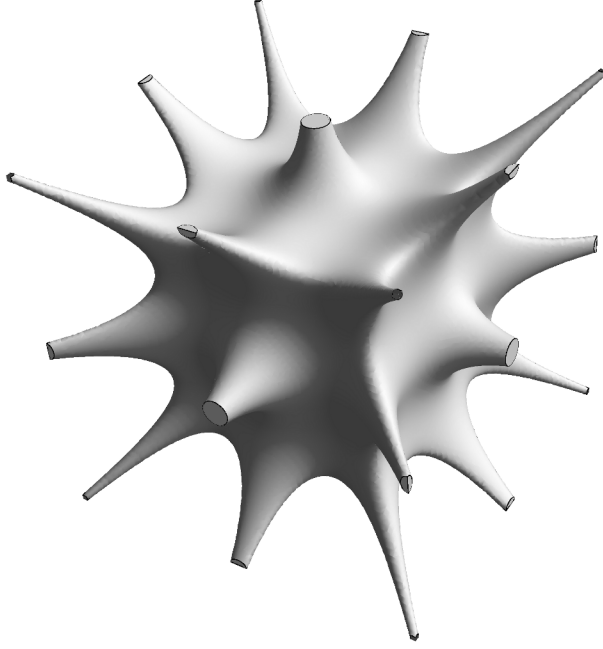


FIG. 12. The flux surface generated from plotting  $\vec{A} = \text{constant}$ . A slice through the centre plane of this surface reproduces the critical flux lines shown in Figure 6. In the limit where the coils are touching, only point cusps are present. As the spacing is increased, the edge cusps span out to the corner cusps and form wide linear loss regions.

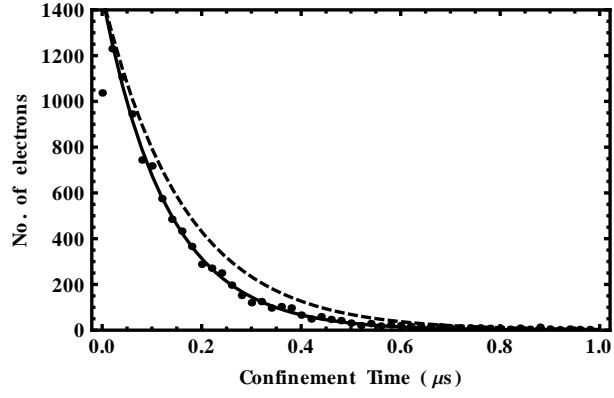


FIG. 13. The distribution of confinement times for 10,000 electron trajectories simulated in the Simion charged particle optics software. The data points have been fitted for the mean confinement time. The theoretical result is shown as the dashed curve.